PHYSICAL REVIEW LETTERS

Surface Induced Phase Separation and Pattern Formation at the Isotropic Interface in Chiral Nematic Liquid Crystals

R. S. Zola,[1,3] L. R. Evangelista,[2] Y.-C Yang,[1] and D.-K. Yang[1]

[1]*Chemical Physics Interdisciplinary Program and Liquid Crystal Institute, Kent State University, Ohio 44242, USA*
[2]*Departamento de Física, Universidade Estadual de Maringá, Avenida Colombo, 5790, 87020-900 Maringá, Paraná, Brazil*
[3]*Universidade Tecnológica Federal do Parana—campus apucarana, Rua Marcílio Dias, 635, 86812-460 Apucarana, Paraná, Brazil*

We study the pattern formation of a chiral nematic liquid crystal under a wetting transition. In the isotropic-liquid crystal transition, a surface-enhanced effect happens and a thin liquid crystal layer forms at the substrates of the cell. In this confined system, chirality, elastic anisotropy, surface anchoring, and wetting strength interplay. A striped pattern is formed due to the chiral nature of the material and the tilted anchoring at the isotropic boundary. As the wetting layer grows from cooling the sample, first the stripes rotate through a process where dislocation defects are formed. As the wetting layer grows further, the periodicity of the stripe structure changes, and finally a splitting of the stripes occurs. Because of the unique properties of this system, new insights about pitch-thickness ratio, interface anchoring, and elastic anisotropy effect are found. Since the anchoring at the isotropic boundary is weak, the critical ratio between the thickness of the wetting layer and the helical pitch is different from that reported in the literature. We also discover that the elastic anisotropy and elastic constant ratios play a critical role in stripe formation. Because of the similarity with biological fibrous composites (twisted plywood), our system may be used as a synthetic version to mimic the naturally occurring one. We carry out a simulation study to explain the experimental results.

PACS numbers: 61.30.Hn, 61.30.−v, 64.70.M−

Introduction.—A solid substrate breaks liquid crystal (LC) bulk symmetry and yields many varieties of interesting phenomena. Among them we shall cite the so-called surface and wetting transitions [1]. The latter occurs when the contact angle of the two coexisting phase becomes zero with respect to a solid substrate when temperature (or composition) is changed [2,3]. The wetting phenomenon has been reported for LCs before [4,5]. In some cases, a LC is filled into a slab cell whose substrates have been coated with a material that favors the nematic phase over the isotropic. This behavior has been well described before for nematics; for details see Ref. [4]. A typical (bulk) isotropic-nematic (IN) transition as described in textbooks is shown in Fig. 1(a). However, for a system consisting of multiple components, in the IN transition, phase separation can be dictated by the surfaces, where the order parameter is higher [6]. Furthermore, confined LC systems, such as the one presented here, are known for presenting distinct physical effects and unique patterns [7–14]. In this Letter, we report the wetting phenomenon of a chiral nematic LC in a slab whose surfaces are coated with an alignment layer of PI2555 (which produces homogeneous alignment parallel to the substrate). Under these conditions, a thin LC layer forms at the substrates separating the surface from the bulk isotropic phase, yielding a confined system where chirality, elastic anisotropy, surface anchoring, and wetting strength interplay to determine the LC orientation. Thus, a study of the chiral nematic anchoring at the isotropic interface is possible. As reported before [15], LCs orient with a

certain inclination (perpendicular to the substrate) at the interface. Under this configuration, the wetting layer forms stripes under appropriate layer thickness, elastic constants, and pitch. This system may be used as a synthetic version to mimic naturally occurring biological fibrous composites [16], also known as twisted plywoods.

Experiments and discussion.—The chiral nematic LC was sandwiched between two parallel glass substrates with cell gap controlled by 10 μm glass fiber spacers. The polyimide (PI2555) was dissolved in a thinner solution with the ratio of 1:8. The material was coated onto the glass substrate, baked, and rubbed to produce a homogeneous alignment. In our experiments, we used four different nematic LC hosts: E44, E7, TL203, and ZLI-4330. They are mixtures consisting of multiple components and exhibit a two-phase region, namely, phase separation, between the isotropic and nematic phase boundary. The physical parameters of these LCs are listed in Table I. The first three had positive dielectric anisotropy whereas the last one had a negative dielectric anisotropy. The chiral dopant used was R811, with a concentration of only a few percent. It did not significantly change the elastic constants and dielectric anisotropy of the nematic hosts because of its low concentration. The cells were studied under polarizing light microscope, and the temperature was controlled with a hot stage where the temperature was lowered at a ratio of 0.3 °C/min.

We first studied the texture of the cell filled with the chiral nematic consisting of 97% E44 and 3% chiral dopant
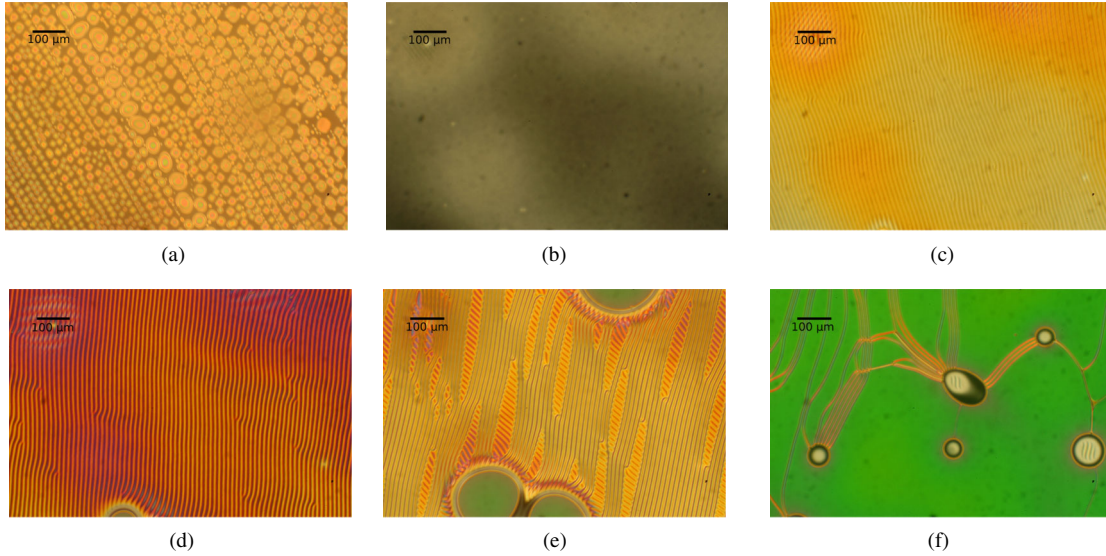
FIG. 1 (color online).   Wetting phenomenon for chiral nematic liquid crystals under cooling of the system from the IN temperature. (a) Nucleation of liquid crystal droplets and (b) beginning of the wetting phenomenon for a chiral nematic cell. [(c) and (d)] Stripes forming as the wetting layer grows. (e) Planar texture nucleating and splitting of the stripes. (f) Planar texture and remaining isotropic domains.

R811 (which generated a pitch of 3.3 μm). The results are shown in Fig. 1. Undergoing the phase transition, the liquid crystalline phase formed first at the surfaces of the cell, as shown in Fig. 1(b). The field of view was brightened gradually with exception of a few defects at the surfaces. At these preliminary states, the LC almost did not twist in the thin wetting layer, and light can be extinguished by changing the rubbing direction of the cell with respect to the crossed polarizers. As the system was further cooled, the wetting layer grew thicker, and light extinction was no longer possible, which indicates the LC orientation was twisted, with the helix axis parallel to the surface normal. However, the twisting rate ϕ/h, (where ϕ is the twist angle and h is the wetting layer thickness) was still small. When the wetting layer reached a critical thickness, it became more favorable to assume an undulated configuration, as shown in Fig. 1(c). This led to a texture of stripes, where the periodicity was approximately equal to the natural pitch of the chiral nematic. Under further cooling, shown in Fig. 1(d), the layer became thicker and the orientation of the stripes rotated with respect to the rubbing direction. At this stage, it was possible to observe many dislocation defects moving quite rapidly in the field of view. As the temperature was further lowered, the planar texture

started to nucleate from spacers and impurities in the cell. The stripes started to split, and stripes with different orientations appeared, corresponding to the stripes formed at the opposite surface, meaning both wetting layers started to have direct contact with each other, as shown in Figs. 1(e) and 1(f). shows the texture when the planar texture took over the entire cell except a little remaining isotropic phase, which was no longer trapped between two LC wetting layers but formed droplets.

The thickness of the wetting layer plays a critical role in the formation of the stripe structure. It is important to know how the thickness of the wetting layer changes with temperature. We ran the following experiment to determine the thickness growth with decreasing temperature. A 20 μm thick cell was filled with the nematic LC E7, and its transmission was measured as a function of temperature. The cell was placed between two crossed polarizers with the LC director making an angle of 45° with the polarizers. We cooled the sample from 62 until 46 °C at 0.5 °C/min, and the transmission was measured using a 632 nm (λ) light. Figure 2 shows that there is a large change of transmission in a narrow temperature interval, from 58 until around 56 °C. The transmission change in this region is associated to the change in thickness of the liquid crystalline wetting layer at the surfaces. Below 56 °C, the change of the transmission is due to the change of the birefringence as a function of temperature. In the transition region, the transmission is given by $T = \sin[2\pi\Delta n(2d)/\lambda]$, where d is the wetting layer thickness (note there are two wetting layers, one on the bottom surface and the other on the top surface of the cell). The layer thickness was calculated from the transmission, and the result is shown by the inset in Fig. 2. The value of the

TABLE I.   Physical parameters of liquid crystals.

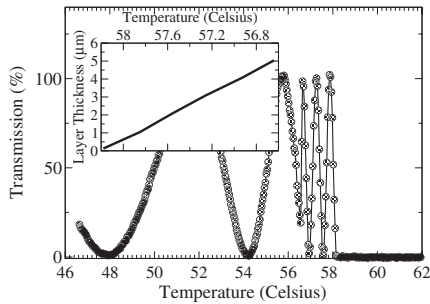| Liquid crystal	K_{11}/K_{22}	K_{33}/K_{22}	$\Delta\varepsilon$
E44	1.19	2.15	17.0
E7	1.48	2.28	13.8
TL203	1.97	2.23	11.0
ZLI-4330	2.00	2.92	−1.9

FIG. 2.　Transmission vs temperature. The large change of the transmission in a narrow interval right after the transition from isotropic phase shows the change in birefringence due to the change in thickness of the wetting layer.
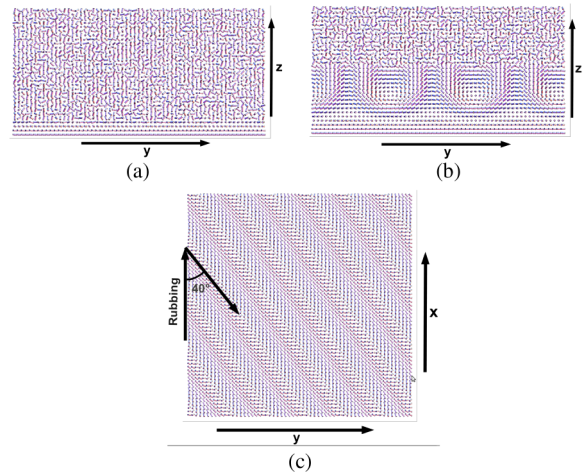

FIG. 3 (color online).　Cholesteric layer growth simulation against isotropic interface; (a) and (b) show the zy plane whereas (c) shows the xy or top view. In (a), the wetting layer is too thin, and no stripes are seen. After a while, stripes develop from the isotropic boundary, as shown in (b). In (c), the period is approximately equal to the natural pitch of the sample.

birefringence Δn was obtained from the literature [17]. The layer grew from 0 to 5 μm in approximately 2 °C.

The bulk free energy involved has two parts: the free energy associated with the orientational order and the elastic energy associated with the nonuniform spatial orientation of the LC director. The surface free energy also has two parts: the anchoring energy at the alignment layer surface, which is strong and does not change much in the narrow temperature range, and the anchoring energy at the LC-isotropic interface, which is weak and changes with the orientation of the LC at the interface. The director configuration within the wetting layer is the state that minimizes the total free energy (bulk free energy plus surface free energy). Experiments have shown that the anchoring strength at a LC-isotropic interface is weak and on the order of 10^{-7} to 10^{-6} J/m^2 [15] and the tilting angle ranges from 50° to 70° with respect to the interface normal [15], which has been verified theoretically [18]. Furthermore, it has been reported before that chiral nematics tend to develop stripes at free surfaces [19,20]. Moreover, stripe domains or fingerprints have been extensively studied before [21,22].

We performed computer simulations and found that the anchoring at the LC-isotropic interface is responsible for the stripe pattern. We used the relaxation method in the Q-tensor representation, which takes into account the symmetry of the chiral nematic phase. This method consists in numerically solving the LC torque balance equation when the free energy is written in the Landau–de Gennes's Q-tensor representation [23,24]. The equations are discretized in a three-dimensional mesh, and at each time step the director is calculated [25]. In the simulation, the anchoring energies were 10^{-4} J/m^2 at the alignment layer (bottom) surface and 10^{-6} J/m^2 at the isotropic (top) surface. The pretilt angle is 88° (with respect to the cell normal) at the bottom surface and 50° at the isotropic interface. We set the initial thickness to 0.3 μm and the initial orientation planar. From the initial orientation, we get the stable configuration by relaxing the LC director. We then increased the thickness stepwise until the LC layer reached 3 μm. After each small change in thickness, we allowed

the free energy of the system slowly to relax to the stable state in a small time step controlled by the relaxation parameter $\alpha = 0.05$ [24]. In every step, a small noise was added to recreate thermal agitation. We chose the x and y lengths equal to 6 μm, while the growing thickness was set in the z direction. Periodic boundary conditions were used in the x and y directions. Figure 3 shows the resulting texture of our simulation where E44's elastic constants ratios are $K_{11}/K_{22} = 1.19$ and $K_{33}/K_{22} = 2.15$ and the pitch is 3 μm. In the initial states, while the LC layer is thin, it has a planar twisted structure with its helical axis uniformly aligned along the z direction, as in Fig. 3(a). In this state, the elastic energy is low and the surface energy at the top surface is high. When the LC layer increases to a certain critical thickness, the LC director assumes an undulated configuration, shown in Figs. 3(b) and 3(c) shows the top view of the LC director configuration on the xy plane. In this undulated state, the surface energy at the top surface is reduced while the elastic energy is increased due to the introduction of the splay and bend deformations. The increase of the elastic energy is less (when the wetting layer is sufficiently thick) than the decrease of the surface energy. The stripe pattern obtained in the simulations is similar to the pattern observed in our experiments, with period approximately equal to the natural pitch, since the anchoring does not allow half-pitch periodicity [26].

We then experimentally studied the pattern formation in the cells with different LCs and found that for long pitches ($h/p< \approx 1$), chiral nematics with E44 and E7 formed stripes whereas chiral nematics with TL203 and ZLI-4330 did not. In order to explain the different behavior, we performed a simulation study on the effect of the ratio between the elastic constants. It was found that when the

ratio of K_{11}/K_{22} is large, the stripe configuration costs too much elastic energy and therefore cannot form. When $h/p = 3$, the ratio must be lower than 1.6 in order to have the stripe structure. The tilted orientation at the interface and the planar orientation in the bottom cause a splay distortion near the interface. If $K_{11} > 1.6K_{22}$, it is too energetically expensive to endure the splay distortion, in such a way that a twist deformation (pitch length change) "pays" the elastic penalty. On the other hand, if $K_{11} < 1.6K_{22}$, the splay distortion will propagate to the bulk. To get rid of this energy, the cholesteric assumes the undulated organization. The pitch length change also explains why the stripes are observed for shorter pitches for all the materials, since the twist energy in cholesterics is inversely proportional to the pitch and therefore has a greater energy cost. As shown in Table I, the ratios of elastic constants are small for E44 and E7 and large for TL203 and ZLI4330. Therefore, the stripe structure forms in the cells with E44 and E7 but not in the cells with TL203 and ZLI4330. The simulated LC director configurations in the cells with E44 and TL203 are shown in Fig. 4. In these figures, the color of the background shows the energy density. The darker color represents higher density of energy. In the cell with E44, the elastic energy density is high in the bulk whereas in the cell with TL203 the surface energy is higher at the top (isotropic) surface.

We also studied the effect of the helical pitch p. It is well-known that the ratio h/p determines the transition of nematic to chiral nematic in homeotropic oriented cells and hybrid aligned cells, where $h/p = 1$ is the critical thickness [27,28]. We experimentally observed that when the pitch was sufficiently short (< 1 μm), the cells with all of the four types of LCs exhibited the stripe texture. We performed a simulation study of the effect of pitch in the cell with the weak anchoring. The result shows that for E44 the critical value of the ratio h/p is 0.7 above the ratio at which the stripe structure forms. For E7, the critical value of the ratio h/p is 1.7 because its value of $K_{11}/K_{22} = 1.48$, which is higher than that of E44. The measured value of h/p is, however, smaller, probably due to the fact that there are nucleation seeds produced by irregularities, such as impurity and spacers, in the cells. When the pitch is shorter, the strips form continuously everywhere in the sample [22].

One interesting feature of the stripes is that the stripes' direction constantly rotates as the cell is cooled. Similar

behavior has been reported for wedge cells under electric fields [28]. This is a direct consequence of the molecular reorientation in the middle of the cell and the change in thickness due to the growth of the wetting layer. As suggested in Ref. [28] (where hybrid aligned chiral nematics in wedge cells were studied), the rotation of the stripes should be related to the helical structure near the planar substrate even after the stripe domains are formed. The fact that the anchoring at the isotropic interface is weak makes it easier for the stripes to rotate. The microphotographs taken at four different temperatures are shown in Fig. 5(a), where the LC was E7 with 1.6% of R811 in a 5 μm cell. The stripes rotated clockwise (chiral dopant sense) with decreasing temperature [29]. The angle of the stripe with respect to the rubbing direction decreased with decreasing temperature as shown in Fig. 5(b). The rotation direction always follows the chiral dopants' handedness. We ran a simulation to investigate the rotation of the stripes. The result shows that as the wetting layer thickness increases with cooling temperature, the thickness of the planar layer between the bottom surface and the top stripe region, as shown in Fig. 3(b), increases. Note that when the wetting layer grows, the thickness of the stripe structure remains constant while the thickness of the planar layer increases. The orientation of the LC molecules at the bottom of the planar layer is fixed by the bottom alignment layer with the strong anchoring strength, whereas the LC molecules at the top of the planar layer tend to rotate such that the pitch length remains the same as the natural pitch as the layer is growing. The orientation of the molecules at the top of the planar layer makes the stripes rotate, because the isotropic surface imposes little resistance. As shown by the inset in Fig. 5(b), the angle of the stripes is linearly related to the thickness of the wetting layer.

To conclude, we studied the surface wetting of chiral nematic liquid crystals consisting of multiple components. In the isotropic-chiral nematic phase transition, they phase separated into an isotropic layer and LC layer. The LC layer is on the surface of the homogeneous alignment layer
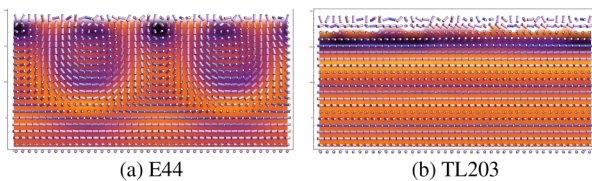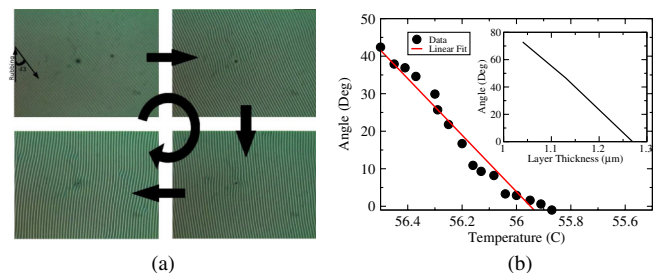

(a)

(b)

FIG. 4 (color online).   (a) and (b) Wetting layer with E44 and TL203, respectively. As in the experiment, the stripe pattern is observed for E44 but not for TL203.

FIG. 5 (color online).   (a) Stripe rotation as the wetting layer grows. When the stripes first appear, they are oriented to an angle of 43° with the rubbing direction. As the system is cooled, the stripes continually rotate and the periodicity increases. (b) Stripe direction with respect to the rubbing direction at different temperatures, whereas the inset shows the simulated results (angle vs layer thickness).

made from PI2555. As the temperature was decreased, the LC layer grew, which made it possible to have a variety of structures. We found that the elastic anisotropy and the elastic constant ratios are decisive for the pattern formation and that the critical ratio h/p is smaller than 1, which is different from that reported in the literature.

[1] S. Aya, K. V. Le, Y. Sasaki, F. Araoka, K. Ishikawa, and H. Takezoe, Phys. Rev. E **86**, 010701(R) (2012); S. Dhara, J. K. Kim, S. M. Jeong, R. Kogo, F. Araoka, K. Ishikawa, and H. Takezoe, Phys. Rev. E **79**, 060701 (2009); G. Ryschenkow and M. Kleman, J. Chem. Phys. **64**, 404 (1976); J. S. Patel and H. Yokoyama, Nature (London) **362**, 525 (1993); V. G. Nazarenko and O. D. Lavrentovich, Phys. Rev. E **49**, R990 (1994); A. C. McUmber, P. S. Noonan, and D. K. Schwartz, Soft Matter **8**, 4335 (2012).

[2] H. Nakanishi and M. E. Fisher, Phys. Rev. Lett. **49**, 1565 (1982).

[3] J. W. Cahn, J. Chem. Phys. **66**, 3667 (1977).

[4] H. Yokoyama, S. Kobayashi, and H. Kamei, Mol. Cryst. Liq. Cryst. **99**, 39 (1983).

[5] N. M. Silvestre, Z. Eskandari, P. Patricio, J. M. Romero-Henrique, and M. M. Telo da Gamma, Phys. Rev. E **86**, 011703 (2012); Y. P. Chiu, C. Y. Shen, W. C. Wang, T. Y. Chu, and Y. H. Lin, Appl. Phys. Lett. **96**, 131902 (2010); B. Alkhairalla, H. Allinson, N. Boden, S. D. Evans, and J. R. Henderson, Phys. Rev. E **59**, 3033 (1999); M. I. Boamfa, M. W. Kim, J. C. Maan, and Th. Rasing, Nature (London) **421**, 149 (2003); C. Poulard, M. Voue, J. De Coninck, and A. M. Cazabat, Colloids Surf. A **282–283**, 240 (2006); J. Daillant, G. Zalczer, and J. J. Benattar. Phys. Rev. A **46**, R6158 (1992).

[6] A. A. Sonin, *Surface Physics of Liquid Crystals* (Gordon and Breach Publishers, New York, 1995).

[7] J. Jeong and M. W. Kim, Phys. Rev. Lett. **108**, 207802 (2012).

[8] L. F. Rull, J. M. R.-Enrique, and A. F.-Nieves, J. Chem. Phys. **137**, 034505 (2012).

[9] D. de L. Heras, E. Velasco, and L. Mederos, J. Chem. Phys. **120**, 4949 (2004).

[10] G. Barbero, L. R. Evangelista, and I. Lelidis, Phys. Rev. E **67**, 051708 (2003).

[11] D. Krzyzanski and G. Derfel, Phys. Rev. E **63**, 021702 (2001).

[12] A. M. Cazabat, U. Delabre, C. Richard, and Y. Y. C. Sang, Adv. Colloid Interface Sci. **168**, 29 (2011).

[13] O. V. Manyuhina, A.-M. Cazabat, and M. B. Amar, Europhys. Lett. **92**, 16005 (2010).

[14] U. Delabre, C. Richard, and A. M. Cazabat, J. Phys. Condens. Matter **21**, 464129 (2009).

[15] S. Faetti and V. Palleschi, Phys. Rev. A **30**, 3241 (1984).

[16] G. De Luca and A. D. Rey, Phys. Rev. E **69**, 011706 (2004).

[17] I. I. Smalyukh, A. N. Kuzmin, A. V. Kachynski, P. N. Prasad, and O. D. Lavrentovich, Appl. Phys. Lett. **86**, 021913 (2005).

[18] R. Holyst and A. Poniewierski, Phys. Rev. A **38**, 1527 (1988).

[19] R. Meister, M.-A. Halle, H. Dumoulin, and P. Pieranski, Phys. Rev. E **54**, 3771 (1996).

[20] J. Baudry, S. Pirkl, and P. Oswald, Phys. Rev. E **57**, 3038 (1998).

[21] P. E. Cladis and M. Kleman, Mol. Cryst. Liq. Cryst. **16**, 1 (1972).

[22] P. Oswald, J. Baudry, and S. Pirkl, Phys. Rep. **337**, 67 (2000).

[23] S. Dickmann, J. Eschler, O. Cossalter, and D. A. Mlynski, SID'93 Dig. 638 (1993).

[24] D.-Ke Yang and S. T. Wu, *Fundamentals of Liquid Crystal Devices* (John Wiley and Sons, New York, 2006), 1st ed.

[25] H. Mori, E. C. Gartland, J. R. Kelly, and P. J. Bos, Jpn. J. Appl. Phys. **38**, 135 (1999).

[26] T. Ishikawa and O. D. Lavrentovich, Phys. Rev. E **60**, R5037 (1999).

[27] F. Lequeux, P. Oswald, and J. Bechhoefer, Phys. Rev. A **40**, 3974 (1989).

[28] T. Nose, T. Miyanishi, Y. Aizawa, R. Ito, and M. Honma, Jpn. J. Appl. Phys. **49**, 051701 (2010).

[29] M. Mathews, R. S. Zola, S. Hurley, D.-Ke. Yang, T. J. White, T. J. Bunning, and Q. Li, J. Am. Chem. Soc. **132**, 18361 (2010).